

# V2X-R: Cooperative LiDAR-4D Radar Fusion with Denoising Diffusion for 3D Object Detection

Xun Huang<sup>123</sup> Jinlong Wang<sup>12</sup> Qiming Xia<sup>12</sup> Siheng Chen<sup>4</sup>  
 Bisheng Yang<sup>5</sup> Xin Li<sup>6</sup> Cheng Wang<sup>12</sup> Chenglu Wen<sup>12\*</sup>

<sup>1</sup>Fujian Key Laboratory of Sensing and Computing for Smart Cities, Xiamen University, China

<sup>2</sup>Key Laboratory of Multimedia Trusted Perception and Efficient Computing,  
 Ministry of Education of China, Xiamen University, China

<sup>3</sup>Zhongguancun Academy <sup>4</sup>Shanghai Jiao Tong University

<sup>5</sup>Wuhan University <sup>6</sup>Texas A&M University

## Abstract

Current Vehicle-to-Everything (V2X) systems have significantly enhanced 3D object detection using LiDAR and camera data. However, they face performance degradation in adverse weather. Weather-robust 4D radar, with Doppler velocity and additional geometric information, offers a promising solution to this challenge. To this end, we present V2X-R, the first simulated V2X dataset incorporating LiDAR, camera, and 4D radar modalities. V2X-R contains 12,079 scenarios with 37,727 frames of LiDAR and 4D radar point clouds, 150,908 images, and 170,859 annotated 3D vehicle bounding boxes. Subsequently, we propose a novel cooperative LiDAR-4D radar fusion pipeline for 3D object detection and implement it with multiple fusion strategies. To achieve weather-robust detection, we additionally propose a Multi-modal Denoising Diffusion (MDD) module in our fusion pipeline. MDD utilizes weather-robust 4D radar feature as a condition to guide the diffusion model in denoising noisy LiDAR features. Experiments show that our LiDAR-4D radar fusion pipeline demonstrates superior performance in the V2X-R dataset. Over and above this, our MDD module further improved the foggy/snowy performance of the basic fusion model by up to 5.73%/6.70% and barely disrupting normal performance. The dataset and code will be publicly available at: <https://github.com/ylwhxht/V2X-R>.

## 1. Introduction

Autonomous driving and other unmanned systems have garnered widespread attention in recent years. This has led to rapid advancements in 3D object detection [4, 24, 65].

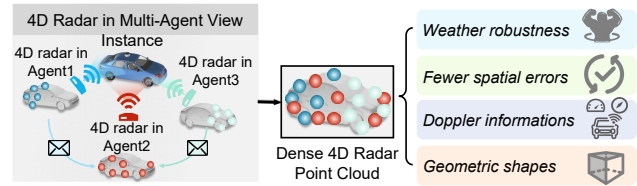


Figure 1. The advantages of the dense 4D radar point cloud in multi-agent view. Including weather robustness, fewer spatial errors, Doppler information, and geometric shapes.

Outdoor environments, however, present complex and dynamic challenges, including various occlusions and weather conditions [14, 45]. Such factors significantly impact the performance of 3D object detection. Consequently, some effort has been made to explore multi-agent cooperative perception, such as vehicle-to-vehicle (V2V), vehicle-to-infrastructure (V2I), and vehicle-to-everything (V2X) [53, 54, 57, 64]. Benefiting from the information shared between agents, in complex outdoor scenarios, cooperative 3D object detection has natural advantages, such as long detection distance and multi-view object observation.

Current research in cooperative 3D object detection mainly focuses on two strategies: LiDAR-based single modality [12, 32, 53, 55, 60] and LiDAR-camera multi-modal fusion [13, 48, 54, 66, 68]. The latter strategy provides more fine-grained information and, therefore, improves the performance of single LiDAR-based methods to some extent. However, both LiDAR point clouds and camera images are weather-sensitive. They are all prone to become noisy in adverse weather [8, 9, 15].

Aside from LiDAR and camera, 4D radar has also been widely noticed [1, 10, 16, 39, 41, 42] because it can perform all-weather sensing and provide speed measurements [67]. Fusing 4D radar and LiDAR is expected to improve the per-

\*Corresponding author, clwen@xmu.edu.cn

ception performance under adverse weather conditions. As shown in Fig. 1, cooperative 4D radar and LiDAR fusion perception have the following advantages:

- *Weather robustness.* The millimeter-wave signals of 4D radar easily penetrates particles in adverse weather [7, 31, 51]. Fusing 4D radar and LiDAR will grant the model weather robust sensing capabilities.
- *Fewer spatial relationship errors.* The error-prone operations (view-transformation or depth-estimation) [1, 43, 44] are not involved in the process of 4D radar and LiDAR point cloud fusing. Thus, there are fewer corresponding spatial relationship errors in fusing 4D radar and LiDAR.
- *Additional Doppler information.* The Doppler information provided by 4D radar is favorable for object detection [1, 16], significantly aiding in the detection of moving objects.
- *Richer geometric shape information.* The multi-agent view can significantly address the limitation of low resolution in 4D radar. This empowers 4D radar’s capacity to complement LiDAR with more geometric shape information of objects.

However, there is a lack of 4D radar data in the current cooperative perception dataset. Therefore, we present V2X-R, the first simulated cooperative 3D Object Detection V2X dataset that not only includes LiDAR, cameras, but also 4D radar data. V2X-R contains 12,079 scenarios with 37,727 frames of LiDAR and 4D radar point clouds, 150,908 images, and 170,859 annotated 3D vehicle bounding boxes. Built upon this dataset, we develop a general cooperative LiDAR-4D radar fusion pipeline for 3D object detection. The entire pipeline consists of four stages: 1) Encode by each agent. 2) Agent fusion. 3) Modal fusion. 4) Box prediction. To address the challenge of agent-fused LiDAR features becoming noisy in adverse weather, we propose a novel Multi-modal Diffusion Denoising (MDD) module in the modal fusion stage of the pipeline. MDD transforms the noise feature distribution into the easy-to-fit Gaussian distribution by reparameterization, which solves the challenge of complex and variable weather noise features that are difficult to fit. It further utilizes weather-robust 4D radar feature as a condition to prompt the diffusion model to denoise noisy LiDAR features. Notably, our MDD module barely disrupts performance in normal weather, attaining high performance in both normal and adverse weather.

Subsequently, we implement the cooperative LiDAR-4D radar fusion pipeline with various agent fusion and modal fusion strategies on our V2X-R dataset, establishing a comprehensive benchmark for cooperative 3D object detection. The comprehensive experiment results show that the LiDAR-4D radar fusion demonstrates superior performance based on various model architectures, as shown in Fig. 2(a). The effectiveness of our designed MDD module is also validated under noise-prone foggy and snowy weather.

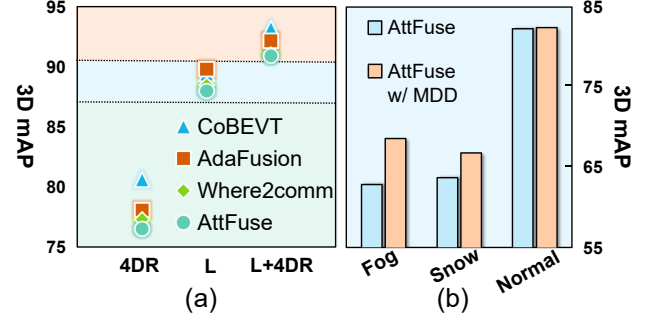


Figure 2. The performance of different methods in our V2X-R dataset. (a) Performance comparison of different modalities (L and 4DR represent LiDAR and 4D radar modality, respectively). (b) Performance comparison of AttFuse [54] model (with and without our MDD module) under different weather conditions.

As shown in Fig. 2(b), by incorporating our MDD module, AttFuse [54] has significantly improved the weather-robustness ability.

Our contributions can be summarized in three key points:

- We present V2X-R, the first simulated V2X dataset that not only includes LiDAR, cameras, but also 4D radar data. This dataset lays the data foundation for research in V2X cooperative perception with 4D radar.
- We designed a novel Multi-modal Diffusion Denoising (MDD) module to utilize reparameterization and weather-robust 4D radar feature to handle hard-to-fit noisy LiDAR feature. Our MDD shows effectiveness in both single and multi-agent, simulated and real scenarios.
- We construct a cooperative LiDAR-4D radar fusion pipeline for 3D object detection. We have implemented this pipeline with various fusion strategies and provided a comprehensive benchmark on our V2X-R dataset, boosting the research in cooperative LiDAR-4D radar fusion for cooperative 3D object detection.

## 2. Related Work

### 2.1. 3D Object Detection

3D object detection has garnered significant attention, with mainstream approaches categorized as LiDAR-based [3, 18, 36, 37, 40, 46, 47, 59, 61, 65] or LiDAR-camera fusion-based [20, 24, 43, 44, 58]. The latter achieves superior performance by combining LiDAR’s depth and geometry information with the fine-grained details from images. However, LiDAR’s weather sensitivity leads to poor performance in adverse conditions, prompting research into weather-robust 3D object detection methods [8, 15, 23]. Some approaches utilize weather-robust 3D Radar [21, 22, 31, 38] or 4D radar [1, 16, 41, 42] fusion with LiDAR. 4D radar has received more attention due to higher resolution and elevation, but cooperative LiDAR-4D radar fusion remains unexplored.

## 2.2. Cooperative Perception Datasets

Large-scale multi-sensor cooperative perception datasets, such as V2V4Real [56], are crucial for training robust and generalizable perception models. However, real-world data collection is costly and time-consuming. Simulation platforms like CARLA [6], SUMO [25], and OpenCDA [52] offer a cost-effective alternative. Datasets such as OPV2V [54] and V2X-Sim [19] have been developed using these tools, supporting tasks like 3D object detection, tracking, and bird's-eye view (BEV) segmentation. However, above datasets lack of 4D Radar data, which limits the research of model robustness under adverse weather conditions.

## 2.3. V2X Cooperative Perception

V2X cooperative perception enhances semantic understanding by sharing observations from surrounding vehicles and infrastructure. Research can be categorized into early fusion [2], mid fusion [12, 53–55, 60], and late fusion [33, 34, 63]. Mid fusion, involving feature sharing among connected and automated vehicles (CAVs), is favored for its performance-bandwidth balance [60]. Most methods are LiDAR-based, with advancements such as self-attention for feature fusion [54], unified Transformer structures for heterogeneous data [53], and bandwidth optimization [12]. For LiDAR-camera fusion, BM2CP [66] proposes a multi-modal cooperative perception framework, while CodeFilling [13] facilitates perception-communication trade-offs. However, the weather sensitivity of LiDAR and camera sensors still poses challenges for multi-agent 3D object detection.

## 3. V2X-R Dataset

### 3.1. Simulator Selection

We chose CARLA [6] as the primary simulator for data collection. Our data is derived from the eight towns provided by CARLA. However, since CARLA lacks vehicle-to-everything (V2X) communication and cooperative driving capabilities, we used OpenCDA [52] integrated with CARLA, a cooperative simulation platform that supports multiple cooperative agents and basic control over embedded vehicular network communication protocols, to generate our V2X-R dataset. Additionally, we integrated the simulated 4D radar sensor into the OpenCDA framework for 4D radar simulation and data collection.

### 3.2. Sensor configuration

As described in Table 1, each Connected Autonomous Vehicle (CAV) and Infrastructure is equipped with four cameras; a 64-channel LiDAR sensor featuring a detection range of 120 meters; a radar sensor with a vertical field of view of 30 degrees and a maximum detection range of 150 meters. The vehicle is equipped with a Global Navigation Satellite System (GNSS) with an altitude noise of 0.001 meters, while

Sensors	Details
4x Camera	4 units RGB, Positions: (2.5,0,1.0,0),(0.0,0.3,1.8,100), (0.0,-0.3,1.8,-100), (-2.0,0.0,1.5,180)
1x LiDAR	64 channels, 120m range, -25° to 2° vertical FOV, 0.02 noise standard deviation, 20 Hz rotation frequency
1x 4D radar	150m range, 120° horizontal FOV, 30° vertical FOV
GPS & IMU	Vehicle GNSS: altitude noise 0.001m; Vehicle IMU: heading noise 0.1°, speed noise 0.2m/s; RSU GNSS: altitude noise 0.05 m,

Table 1. Sensor configuration details of our V2X-R dataset.

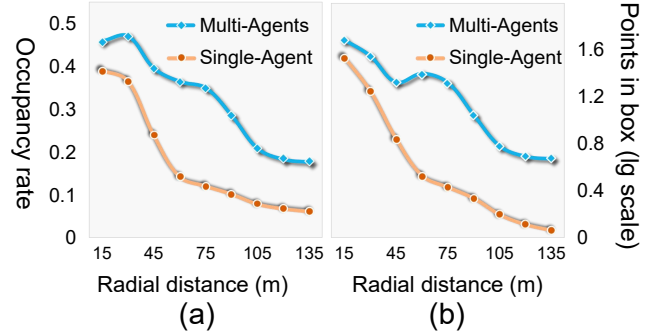


Figure 3. 4D radar point cloud occupancy rate (a) and number of points (b) within the ground truth bounding boxes for radial distance from ego vehicles.

the roadside unit (RSU) has an altitude noise of 0.05 meters. Finally, based on the above configuration, our V2X-R contains a total of 12,079 scenarios with 37,727 frames of LiDAR and 4D radar point clouds, 150,908 images, and 170,859 annotated 3D vehicle bounding boxes.

### 3.3. Cooperative 4D Radar Point Cloud Analysis

We analyzed the instance occupancy and points of the 4D radar point cloud before and after the multi-agent cooperative communication, as shown in Fig. 3. The 4D radar point cloud instance occupancy and points at different distances increase significantly with multi-agent collaboration. Especially in the middle and long distance, 4D radar point clouds can still have relatively high instance occupancy and points. These data demonstrate the independent perception capability of the cooperative 4D radar point cloud.

### 3.4. Adverse Weather Simulation

To analyze the performance under adverse weather conditions on our V2X-R dataset, we applied fog [8] and snow [9] simulations to the LiDAR point clouds based on physical reflection and geometric optics method. Recent research [5, 31] has confirmed the consistency of perception performance between simulated and real-world adverse weather data. Detailed implementations of fog and snow simulations will be introduced in the supplementary material.

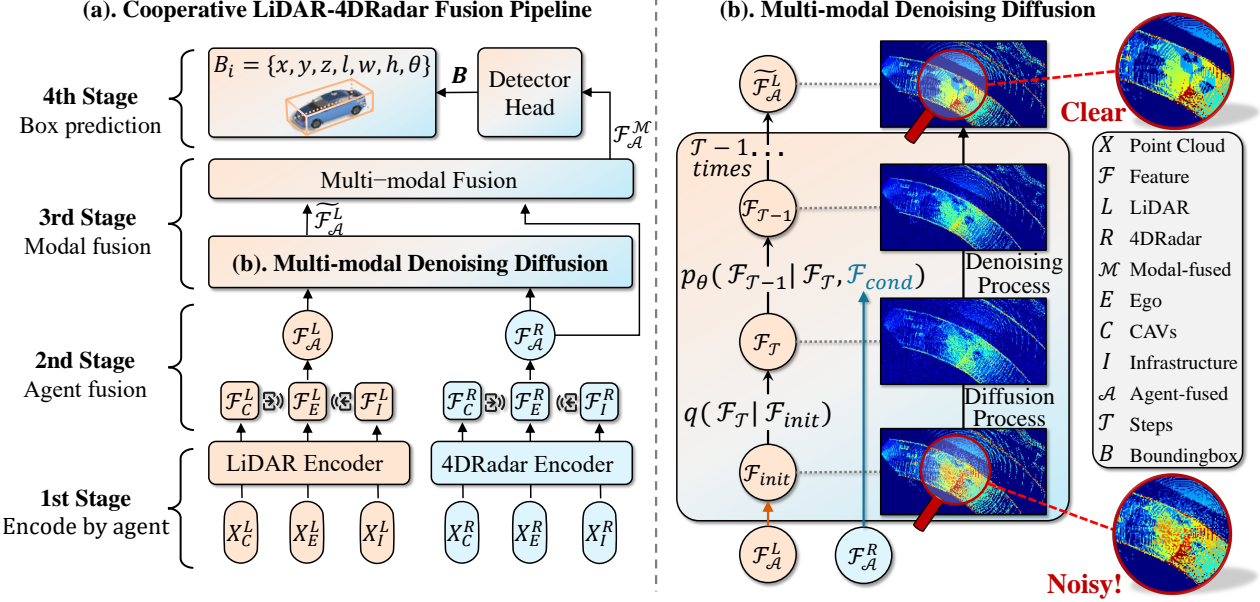


Figure 4. The pipeline of constructed cooperative LiDAR-4D radar fusion for weather-robust 3D object detection. The fusion pipeline (a) is first fed with multi-modal point cloud (LiDAR and 4D radar) from multi-agent: Ego Vehicle (E), Connected Automated Vehicle (C), and Infrastructure (I). Subsequent fusion consists of four stages: 1) Encode by each agent. 2) Agent fusion. 3) Modal fusion. 4) Box prediction. Additionally, a Multi-modal Denoising Diffusion (b) module is integrated into the pipeline to achieve weather-robust ability. The input noisy LiDAR features are first subjected to a diffusion process, followed by  $\mathcal{T}$  step denoising process with weather-robust 4D radar features as conditions to get the denoised clear LiDAR features.

## 4. Cooperative LiDAR-4D Radar Fusion

### 4.1. Overall Statement

Built upon the V2X-R dataset, we present the first exploration of cooperative LiDAR-4D radar fusion for 3D object detection. To the best of our knowledge, no prior work has investigated this problem. In sec. 4.2, we introduce the first cooperative LiDAR-4D radar fusion pipeline for weather-robust 3D object detection. Furthermore, in sec. 4.3, we enhance the weather-robustness of cooperative LiDAR-4D radar fusion by leveraging the advantage of 4D radar in adverse weather conditions. We analyze the strengths and challenges of cooperative LiDAR point clouds in adverse weather conditions and propose the Multi-modal Denoising Diffusion (MDD) module to tackle these challenges, significantly improving the pipeline’s weather-robustness.

### 4.2. Fusion Pipeline

In the cooperative LiDAR-4D radar fusion pipeline, there are three types of agents: Ego Vehicle (E), Connected Automated Vehicle (C), and Infrastructure (I). Each agent collects LiDAR and 4D radar point cloud data, forming the multi-agent multi-modal input  $\mathbf{X} = \{X_C^L, X_E^L, X_I^L, X_C^R, X_E^R, X_I^R\}$ . As illustrated in the Fig. 4(a), subsequent fusion consists of four stages:

1) *Encode by agent*. We feed  $\mathbf{X}$  into a agent-shared en-

coder  $\mathcal{G}_\theta$  to obtain features for each agent and modality as:

$$\mathcal{F}_j^i = \mathcal{G}_\theta(X_j^i), \quad (1)$$

where  $i \in \{L, R\}$  denotes modality and  $j \in \{C, E, I\}$  denotes agent.

2) *Agent fusion*. After encoding, the features with same modality in different agent  $\{\mathcal{F}_C^i, \mathcal{F}_E^i, \mathcal{F}_I^i | i \in \{L, R\}\}$  communicate with each other, the agent-fusion  $\phi_A$  is performed to get multi-agent feature  $\mathcal{F}_A^i$  for  $i$  modality as:

$$\mathcal{F}_A^i = \phi_A(\mathcal{F}_C^i, \mathcal{F}_E^i, \mathcal{F}_I^i). \quad (2)$$

3) *Modal fusion*. The weather-induced noisy LiDAR feature  $\mathcal{F}_A^L$  will first be denoised to clear LiDAR feature  $\tilde{\mathcal{F}}_A^L$  by MDD module (will be described in the next section). Then, we perform modal-fusion  $\phi_M$  to obtain the multi-agent multi-modal features  $\mathcal{F}_A^M$  as:

$$\mathcal{F}_A^M = \phi_M(\tilde{\mathcal{F}}_A^L, \mathcal{F}_A^R). \quad (3)$$

4) *Box prediction*. Finally, we use the detector head to predict the 3D bounding box  $\mathbf{B}$  by using the multi-agent multi-modal features  $\mathcal{F}_A^M$ .

The two keys to implementing the above fusion pipeline lie in the agent-fusion and modal-fusion stages. Since there is no cooperative LiDAR-4D radar fusion method available

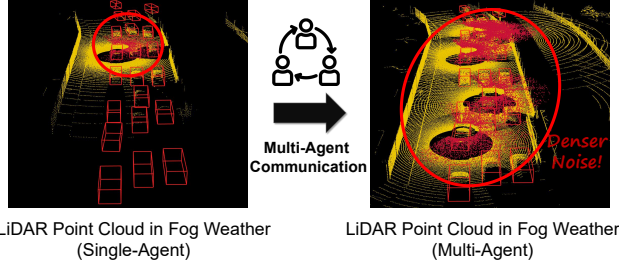


Figure 5. Visualization of LiDAR point cloud under foggy (simulated) weather before and after multi-agent communication. After multi-agent communication, the LiDAR point cloud has a longer vision, but a serious challenge of denser noise (red points).

yet. We explored two implementations that extend the existing mature fusion to cooperative LiDAR-4D radar fusion:

(a) **Single-Agent Multi-Modal to Multi-Agent Multi-Modal (SA2MA).** LiDAR-4D radar fusion in single-agent has received considerable attention [1, 16, 41, 42]. Therefore, we extend existing single-agent LiDAR-4D radar fusion methods to the multi-agent version by integrating a self-attention-based agent-fusion module (2nd stage).

(b) **Multi-Agent Single-Modal to Multi-Agent Multi-Modal (SM2MM).** Another approach is to extend the widely researched multi-agent LiDAR-based methods [12, 32, 53–55] to the multi-modal version. Specifically, we first extract multi-agent features from LiDAR and 4D radar point clouds individually and then concatenate BEV features in multi-modal fusion (3rd stage).

### 4.3. Multi-modal Denoising Diffusion (MDD)

We first analyzed the cooperative LiDAR point cloud in adverse weather. As shown in Fig. 5, single-agent LiDAR point clouds exhibit the effects of reduced detection range and weather noise in fog weather. With multi-agent communication, the effect of reduced detection range is largely solved, but at the same time, weather noises exacerbate as they propagate through communication.

Therefore, addressing the dense noise challenge is crucial for weather-robust 3D object detection. Point-level semantic segmentation for denoising is time-consuming, struggles with intertwined noise and objects, and is incompatible with common multi-agent feature fusion strategies. On the other hand, simple feature-level denoising leads to poor fitting due to the complex distribution of weather noise in the feature. To overcome these limitations, we propose the Multi-modal Denoising Diffusion (MDD) for denoising noisy LiDAR features. As shown in Fig. 4(b), we resampled the complex weather noise distribution to a Gaussian distribution through the diffusion process, and then denoised it with the weather-robust 4D radar feature.

Specifically, drawing inspiration from DDPM [11] and MTL [62], gaussian noise is gradually applied to the init

---

#### Algorithm 1 Multi-modal Denoising Diffusion process

---

**Input:** Training  $\in \{\text{True, False}\}$ ; Noisy LiDAR BEV feature  $\mathcal{F}_{\mathcal{A}}^L$ ; Noise-masked LiDAR BEV feature  $\mathcal{F}_l^L$ ; 4D radar BEV feature  $\mathcal{F}_{\mathcal{A}}^R$ ; Diffusion steps  $\mathcal{T}$ ;

**Output:** Training loss and denoised LiDAR feature  $\tilde{\mathcal{F}}_{\mathcal{A}}^L$

$$\mathcal{F}_{init} \leftarrow \mathcal{F}_{\mathcal{A}}^L$$

$$\epsilon \in \mathcal{N}(0, \mathbf{I}) \quad \triangleright \text{Sample noise}$$

$$\mathcal{F}_{\mathcal{T}} = \sqrt{\bar{\alpha}_t} \mathcal{F}_{init} + \sqrt{1 - \bar{\alpha}_t} \epsilon \quad \triangleright \text{Diffusion process}$$

**for**  $t \leftarrow \mathcal{T}, \mathcal{T} - 1, \dots, 1$  **do**

$$\mathcal{F}_{t-1} = U_{\theta}(\text{Concat}[\mathcal{F}_t, \mathcal{F}_{\mathcal{A}}^R], t) \quad \triangleright \text{Denoising process}$$

**end for**

$$\tilde{\mathcal{F}}_{\mathcal{A}}^L \leftarrow \mathcal{F}_0$$

**if** Training **then**

$$\text{Loss} \leftarrow \mathcal{L}_{MDD}(\tilde{\mathcal{F}}_{\mathcal{A}}^L, \mathcal{F}_l^L) \quad \triangleright \text{Compute loss as in eqs. 8}$$

**return** Loss,  $\tilde{\mathcal{F}}_{\mathcal{A}}^L \quad \triangleright \text{Get loss and denoised feature}$

**else**

**return**  $\tilde{\mathcal{F}}_{\mathcal{A}}^L \quad \triangleright \text{Get denoised clear LiDAR feature}$

**end if**

---

feature  $\mathcal{F}_{init}$  (Initialization is  $\mathcal{F}_{\mathcal{A}}^L$ ) in  $\mathcal{T}$  times step-by-step. Suppose the decayed feature at denoising step  $t$  is  $\mathcal{F}_t$ , the diffusion process  $q$  can be formulated as:

$$q(\mathcal{F}_t | \mathcal{F}_{init}) = \mathcal{N}(\mathcal{F}_t | \sqrt{\bar{\alpha}_t} \mathcal{F}_{init}, (1 - \bar{\alpha}_t) \mathbf{I}), \quad (4)$$

where  $\{\bar{\alpha}_t, t \in \{1, 2, \dots, \mathcal{T}\}\}$  are hyper-parameters. We could directly compute the decayed feature  $\mathcal{F}_{\mathcal{T}}$  through mathematical derivation:

$$\mathcal{F}_{\mathcal{T}} = \sqrt{\bar{\alpha}_{\mathcal{T}}} \mathcal{F}_{init} + \sqrt{1 - \bar{\alpha}_{\mathcal{T}}} \epsilon, \epsilon \sim \mathcal{N}(0, \mathbf{I}). \quad (5)$$

This process transforms the original noise distribution  $\delta_{raw}$  into a Gaussian distribution  $\delta_{gau}$  through a Gaussian reparameterization sampling process as:

$$\delta_{gau} = \sqrt{\bar{\alpha}_{\mathcal{T}}} \delta_{raw} + \sqrt{1 - \bar{\alpha}_{\mathcal{T}}} \epsilon, \quad (6)$$

$\delta_{gau} \sim \mathcal{N}(\sqrt{\bar{\alpha}_{\mathcal{T}}} \delta_{raw}, \sqrt{1 - \bar{\alpha}_{\mathcal{T}}})$  subject to Gaussian distribution, which facilitates the fitting of the denoising model. Subsequently, at each denoising step, we incorporate weather-robust 4D radar features  $\mathcal{F}_{\mathcal{A}}^R$  as a condition to prompt U-Net [35] denoiser  $U_{\theta}$  to predict the denoised feature:

$$\mathcal{F}_{t-1} = U_{\theta}([\mathcal{F}_t, \mathcal{F}_{\mathcal{A}}^R], t), t \in \mathcal{T}, \mathcal{T} - 1, \dots, 1. \quad (7)$$

For the final output after  $\mathcal{T}$  denoising steps, the  $U_{\theta}$  generates the denoised clear LiDAR feature  $\tilde{\mathcal{F}}_{\mathcal{A}}^L = \mathcal{F}_0$ . We present the detailed training and inference pipelines MMD in Algorithm 1. And we compute the loss of MDD as :

$$\mathcal{L}_{MDD} = \mathcal{L}_{MSE}(\tilde{\mathcal{F}}_{\mathcal{A}}^L, \mathcal{F}_l^L) * \gamma(e, \psi), \quad (8)$$

where  $\mathcal{F}_l^L$  is the groundtruth feature extracted from the clear LiDAR point cloud after masking the weather noise,

$e$  is the epoch,  $\psi$  is loss weight and  $\gamma(e)$  is the loss weight that we specifically designed for the MDD module as:

$$\gamma(e, \psi) = (1 - \tanh(\frac{e}{\tau} - \varphi)) * \psi, \quad (9)$$

where  $\tau$  is temperature,  $\varphi$  is offset. It decreases nonlinearly with epoch so that the model pays full attention to the feature denoising task in the early period and the object detection task in the late period.

#### 4.4. Loss Function

We trained models with our MDD by the following losses:

$$\mathcal{L}_{all} = \beta_{cls} \mathcal{L}_{cls} + \beta_{loc} \mathcal{L}_{loc} + \mathcal{L}_{MDD}, \quad (10)$$

where  $\beta_{cls}$ ,  $\beta_{loc}$  are hyper-parameters,  $\mathcal{L}_{cls}$  and  $\mathcal{L}_{loc}$  are classification and localization loss, respectively. All hyper-parameters are detailed in the supplementary material.

### 5. Experiments

#### 5.1. Experimental Details and Metrics

We used 8,084/829/3,166 frames for training/ validation/ testing in our V2X-R dataset, ensuring there is no overlap in the intersection of the training/validation/testing sets. For each frame, we ensure that the minimum and maximum numbers of agents are 2 and 5 respectively. We use Adam optimizer with  $lr = 1e-3$ ,  $\beta_1 = 0.9$ ,  $\beta_2 = 0.999$ . Following [54], we select a vehicle as the ego vehicle for evaluation. Detection performance is evaluated near the ego vehicle in a range of  $x \in [0, 140]m$ ,  $y \in [-40, 40]m$ . We set the broadcast range among CAVs to be 70 meters. In addition, since the 4D radar sensor only provides front-view data, all of our evaluation results are in the camera FOV of the ego vehicle.

#### 5.2. Benchmark Models

We implement various state-of-the-art 3D object detectors on the V2X-R dataset, including different numbers of agents and different modalities. The results of these detectors on three different modalities are also given. The chosen 3D detector models for different modalities are as follows.

**Cooperative LiDAR-based 3D object detectors.** We pick existing method including AttFuse [54], V2XViT [53], CoBEVT [55], CoAlign [26], Where2comm [12], AdaFusion [17], SCOPE [60], MACP [27] and SICP [32] for cooperative LiDAR-based benchmarking analysis.

**Cooperative 4D radar-based 3D object detectors.** Due to the lack of cooperative 4D radar-based methods. We first extend the single-agent 4D radar-based FPA-Net [49] and RTNH [28] to the cooperative 4D radar-based method through self-attention agent fusion in AttFuse [54], marked as  $\dagger$ . For a more comprehensive analysis, we also changed the LiDAR point cloud input for the above cooperative

Method	Publication	3D mAP@Validation (IoU=0.3/0.5/0.7)	3D mAP@Testing (IoU=0.3/0.5/0.7)
V2XViT [53]	ECCV2022	85.0/82.2/64.9	90.1/89.0/77.7
Attfuse [54]	ICRA2022	86.0/82.2/66.9	91.4/89.6/80.2
Where2comm [12]	NeurIPS2023	83.7/80.2/56.8	88.1/86.1/69.2
SCOPE [60]	ICCV2023	76.0/74.7/60.9	81.4/72.9/67.0
CoBEVT [55]	CoRL2023	87.6/84.8/71.0	92.3/89.4/82.5
CoAlign [26]	ICRA2023	86.1/84.6/72.1	89.6/88.9/83.3
AdaFusion [17]	WACV2023	88.1/86.9/75.6	92.7/90.6/84.8
SICP [32]	IRROS2024	81.1/77.6/58.1	84.6/82.2/66.7
MACP [27]	WACV2024	72.8/70.9/60.0	83.7/83.1/75.5

Table 2. Experimental 3D object detection results of various cooperative LiDAR-based methods on the validation and testing of our V2X-R dataset in different IoU (0.3,0.5,0.7).

Method	Publication	3D mAP@Validation (IoU=0.3/0.5/0.7)	3D mAP@Testing (IoU=0.3/0.5/0.7)
PFA-Net $\dagger$ [50]	ITSC2021	76.9/68.0/39.3	85.1/79.9/52.5
RTNH $\dagger$ [29]	NeurIPS2022	71.7/62.2/34.4	73.7/67.7/41.9
V2XViT $\dagger$ [53]	ECCV2022	71.1/64.3/31.1	80.9/73.8/42.7
AttFuse $\dagger$ [54]	ICRA2022	75.3/66.5/36.1	81.8/75.4/48.2
Where2comm $\dagger$ [12]	NeurIPS2023	69.4/62.1/26.6	77.8/72.9/41.5
SCOPE $\ddagger$ [60]	ICCV2023	61.9/59.3/47.9	73.0/71.6/51.6
CoBEVT $\ddagger$ [55]	CoRL2023	78.9/71.9/37.5	86.4/81.2/54.7
CoAlign $\ddagger$ [26]	ICRA2023	65.8/59.2/34.7	76.9/70.2/46.2
AdaFusion $\ddagger$ [17]	WACV2023	77.8/72.5/42.9	82.2/78.1/55.5
SICP $\ddagger$ [32]	IRROS2024	70.1/60.6/32.4	71.5/63.5/33.4

Table 3. Experimental 3D object detection results of various cooperative LiDAR-based methods on the validation and testing of our V2X-R dataset in different IoU (0.3,0.5,0.7). The representations of  $\dagger$  and  $\ddagger$  as described in 5.2.

LiDAR-based method to 4D radar point cloud input to implement cooperative 4D radar-based methods, marked as  $\ddagger$ .

**Cooperative LiDAR-4D radar fusion 3D object detectors.** We implement SA2MA fusion on the InterFusion [42] and L4DR [16] models and SM2MM fusion on the AttFuse [54], CoBEVT [54], V2XViT [54], Where2comm [12], CoAlign [26], AdaFusion [17], SICP [32] models.

To intuitively compare the performance in normal weather differences between modalities, the cooperative LiDAR-4D radar fusion 3D object detectors we implemented in the benchmark section do not incorporate the MDD module. The MDD module will be discussed in subsequent experiments.

#### 5.3. Benchmark Analysis

In the following, we will show and analyze the results of three different modalities on our V2X-R dataset.

**Cooperative LiDAR-based 3D object detectors.** Table 2 depicts the performance of the selected cooperative LiDAR-based 3D object detectors. A large number of combined results from these models validate the reliability of our V2X-R dataset. It is worth noting that the performance of the newest methods (SICP [32], MACP [27]) is not as good as that of earlier methods (e.g. COBEVT [55], CoAlign [26], AdaFusion [17]). This is because these newest methods do not solely focus on mainstream perfor-

Method	Publication	Fusion Strategy	3D mAP@Validation			3D mAP@Testing		
			IoU=0.3	IoU=0.5	IoU=0.7	IoU=0.3	IoU=0.5	IoU=0.7
InterFusion [42]	IROS2023	SA2MA	81.23	77.33	52.93	87.91	86.51	69.63
L4DR [16]	Arxiv2024	SA2MA	84.58	82.75	70.29	90.78	89.62	82.91
V2XViT [53]	ECCV2022	SM2MM	85.23	83.90	69.77	91.99	91.22	83.04
AttFuse [54]	ICRA2022	SM2MM	86.14	84.30	70.72	92.20	90.70	84.60
SCOPE [60]	ICCV2023	SM2MM	78.79	77.96	62.57	83.38	82.89	70.00
Where2comm [12]	NeurIPS2023	SM2MM	87.62	85.58	69.61	92.20	91.00	82.04
CoBEVT [55]	CoRL2023	SM2MM	86.69	85.72	<b>75.93</b>	<b>94.00</b>	<b>93.23</b>	<b>86.68</b>
CoAlign [26]	ICRA2023	SM2MM	87.16	85.54	73.79	92.14	91.21	83.77
AdaFusion [17]	WACV2023	SM2MM	<b>89.24</b>	<b>87.31</b>	74.86	93.10	92.15	85.48
SICP [32]	IROS2024	SM2MM	82.46	79.44	61.51	86.19	84.20	68.15

Table 4. Results of various cooperative LiDAR-4D radar fusion methods on the validation and testing of our V2X-R dataset in different IoUs (0.3,0.5,0.7). SA2MA and SM2MM represent *Single-Agent to Multi-Agent* and *Single-Modal to Multi-Modal* as described in sec. 4.2.

Method	Modality	3D mAP@Snow			3D mAP@Fog			3D mAP@Normal		
		IoU=0.3	IoU=0.5	IoU=0.7	IoU=0.3	IoU=0.5	IoU=0.7	IoU=0.3	IoU=0.5	IoU=0.7
1.L4DR [16]	L	-	-	-	-	-	-	-	-	-
2.L4DR [16]	L+4DR	78.88	75.87	59.10	85.00	80.09	61.48	<b>90.66</b>	<b>89.29</b>	<b>80.42</b>
3.L4DR w/MDD	L+4DR	<b>82.89</b>	<b>80.52</b>	<b>65.80</b>	<b>86.00</b>	<b>81.60</b>	<b>63.66</b>	90.44	89.15	80.36
<i>Improvement (3-2)</i>		+4.01	+4.65	+6.70	+1.00	+1.51	+2.18	-0.22	-0.14	-0.06
1.AttFuse [54]	L	62.48	61.53	51.11	74.10	71.35	57.30	87.14	85.00	74.40
2.AttFuse [54]	L+4DR	79.63	77.37	63.71	85.00	80.64	62.89	<b>91.77</b>	<b>90.43</b>	82.22
3.AttFuse w/MDD	L+4DR	<b>83.78</b>	<b>81.19</b>	<b>66.86</b>	<b>87.37</b>	<b>83.90</b>	<b>68.64</b>	91.61	90.27	<b>82.43</b>
<i>Improvement (2-1)</i>		+17.15	+15.84	+12.60	+10.90	+9.29	+5.59	+4.63	+5.43	+7.82
<i>Improvement (3-2)</i>		+4.15	+3.82	+3.15	+2.37	+3.26	+5.73	-0.16	-0.10	+0.21

Table 5. The 3D mAP performance comparison under different weather conditions on the V2X-R dataset. 'L' and '4DR' represent LiDAR and 4D radar, respectively. '-' indicates that multi-modal method L4DR [16] cannot achieve LiDAR-based performance.

mance: SICP emphasizes preserving the ability of individual perception, while MACP employs transfer fine-tuning instead of retraining to avoid the overhead.

**Cooperative 4D radar-based 3D object detectors.** We also pioneered the exploration of cooperative 4D radar-based methods on the V2X dataset. As shown in Table 3, the performance of 4D radar-based models is generally lower than that of LiDAR-based models in Table 2. This can be attributed to the significantly lower resolution of 4D radar than LiDAR, which is a limitation hindering the independent use of 4D radar in single-agent scenarios. However, we also observed that cooperative 4D radar-based methods can achieve the excellent performance of 86.4% 3D mAP@testing (IoU=0.3) (CoBEVT<sup>‡</sup> [55]). This shows that 4D radar can achieve independent perception through cooperative communication, proving the research significance of the cooperative 4D radar-based approach.

**Cooperative LiDAR-4D radar fusion 3D object detectors.** Finally, we implemented and evaluated a series of cooperative LiDAR-4D radar fusion methods following the methodology described in sec. 4.2. As shown in Table 4, by comparing with Tables 2 and 3, it can be observed that

cooperative LiDAR-4D radar fusion achieves the best performance compared to other single-modality approaches. For example, V2XViT [53], AttFuse [54], and CoBEVT [55] exhibit 5.34%, 5.80%, and 4.18% 3D mAP@testing (IoU=0.7) improvements through LiDAR-4D radar fusion, respectively. These results convincingly validate that cooperative 4D radar can bring considerable performance enhancements to the LiDAR single-modality approach.

#### 5.4. Multi-modal Diffusion Denoising Analysis

To explore the weather-robust advantages of 4D radar, we investigated the performance of the LiDAR-4D radar fusion model and verified the effectiveness of our designed MDD module. We trained models by randomly sampling LiDAR point clouds in [normal, fog] for each frame to test on various weather domains: normal weather domain, seen (fog) and unseen (snow) adverse weather domain.

**Performance comparison under different simulated weather on V2X-R dataset.** We selected three models, AttFuse [54] and L4DR [16], which include SA2MA and SM2MM fusion strategies, to evaluate the performance under different weather conditions. As shown in Table 5, the

Class	Method	All	Adverse	Normal
Sedan	AttFuse <sup>†</sup> [54]	69.04	70.72	66.75
	AttFuse <sup>†</sup> w/ MDD	<b>74.03</b>	<b>75.90</b>	<b>67.18</b>
Bus	AttFuse <sup>†</sup> [54]	50.95	48.78	<b>53.33</b>
	AttFuse <sup>†</sup> w/ MDD	<b>54.58</b>	<b>54.75</b>	52.81

Table 6. The 3D mAP performance comparison on K-Radar [28] dataset. Adverse represents average results under various adverse weather, including overcast, fog, rain, sleet, light and heavy snow. <sup>†</sup> represents AttFuse [54] is implemented as single agent method by removing the agent fusion module.

Vanilla-Unet	Diffusion Denoise	4D radar Condition	3D mAP@Fog		
			IoU=0.3	IoU=0.5	IoU=0.7
✓			85.00	80.64	62.89
	✓		85.44	81.23	62.07
	✓		86.41	83.29	68.08
	✓	✓	<b>87.37</b>	<b>83.90</b>	<b>68.64</b>

Table 7. Effect of each component in MDD module, tested by AttFuse [54] on V2X-R testing with fog-simulation.

LiDAR-4D radar fusion can achieve superior performance in various weather conditions. AttFuse achieved 17.17% 3D mAP@snow (IoU=0.3) improvement when compared to LiDAR-only (*Improvement (2-1)*), respectively. Moreover, our designed MDD module improved the basic LiDAR-4D radar fusion model performance by up to 5.73% (AttFuse, 3D mAP@fog) and 6.70% (L4DR, 3D mAP@snow) under adverse weather conditions. Meanwhile, our MDD module hardly affects the normal weather performance, which validates the effectiveness and reliability of our MDD module.

**Performance comparison under different real-world weather on K-Radar dataset.** We further conducted experiments on the K-Radar single-agent real-world dataset. As shown in Table 6, our MDD module demonstrates significant performance improvements in real-world adverse weather, with 3D mAP gains of 5.20% and 5.97% for the Sedan and Bus classes, respectively. Consistent with the results on V2X-R dataset, MDD has rarely impacted the normal weather performance, resulting in overall improvements of 4.99% and 3.63%. These results validate the effectiveness of the MDD module in the presence of dense noise under adverse weather, whether single or multi-agent perception. Detailed evaluation metrics and performance of each weather can be found in the supplementary materials.

**Effect of each component.** We systematically evaluated each component, with the results summarized in Table 7. We initially attempted to denoise LiDAR features using Vanilla-Unet (row 2<sup>st</sup>) but found the results unsatisfactory. The complex distribution of LiDAR noise in multi-agent settings is difficult to directly fit. We significantly

Diffusion Layers	Loss Weight	Inference Speed	3D mAP@Fog		
			IoU=0.3	IoU=0.5	IoU=0.7
-	-	18 ms	85.00	80.64	62.89
$\mathcal{T} = 2$	1	39 ms	85.85	82.19	65.47
	3		86.68	82.77	65.92
	5		85.54	81.79	65.89
	$\gamma(e, \psi = 1)$		86.98	83.31	66.91
	$\gamma(e, \psi = 3)$		87.35	83.78	68.14
	$\gamma(e, \psi = 5)$		86.91	83.46	66.99
$\mathcal{T} = 3$	3	50 ms	85.97	82.43	66.23
	$\gamma(e, \psi = 3)$		<b>87.37</b>	<b>83.90</b>	<b>68.64</b>
$\mathcal{T} = 4$	3	59 ms	86.98	83.15	65.13
	$\gamma(e, \psi = 3)$		87.01	83.89	67.58

Table 8. Effect of diffusion layers and loss weight in MDD module, tested by AttFuse [54] on V2X-R testing with fog-simulation.

improve performance by transforming the noise distribution into Gaussian distribution through a multi-step diffusion process (row 3<sup>rd</sup>). Finally, by incorporating weather-robust 4D Radar features as conditional information for multi-modal denoising (row 4<sup>th</sup>), the model achieves the best performance of 87.37/83.90/86.64 3DmAP@Fog.

**Effect of diffusion layers and loss weight.** Finally, we investigate the impact of diffusion layers  $\mathcal{T}$  and the loss weight of MDD in our MDD module. Table 8 presents representative results. We first explore the MDD loss weight with  $\mathcal{T} = 2$ , considering both constant weights and the epoch-varying weight  $\gamma(e, \psi)$  in eqs. 9. The best performance is achieved with  $\gamma(e, \psi = 3)$  when  $\mathcal{T} = 2$ . We further experiment with different values of  $\mathcal{T}$ . When  $\mathcal{T} = 2$  and the loss weight is  $\gamma(e, \psi = 3)$ , our MDD module achieves the best performance of 87.37/83.90/86.64 3DmAP@Fog. Although MDD inevitably introduces an additional inference time of 32 ms, it significantly improves weather robustness and still maintains real-time (about 20 FPS). These results validate the effectiveness of our designed weight  $\gamma(e, \psi)$  and real-time of our MDD module.

## 6. Conclusion and Discussion

We present V2X-R, the first simulated V2X collaborative perception dataset incorporating 4D radar. We establish a benchmark on V2X-R dataset by integrating a LiDAR-4D radar fusion pipeline into classic collaborative 3D object detection methods. Moreover, we propose the MDD module to tackle dense noise in collaborative conditions. In summary, V2X-R and our exploration paves the way for advancing collaborative LiDAR and 4D radar fusion perception.

**Limitations and future work.** While our work provides a strong foundation, deeper exploration of cooperative LiDAR and 4D radar fusion remains underdeveloped. A compelling research direction is the full utilization of multi-agent and multi-modal information for more robust 3D object detection.

# V2X-R: Cooperative LiDAR-4D Radar Fusion with Denoising Diffusion for 3D Object Detection

## Supplementary Material

### 7. Additional Details of V2X-R Dataset

Here we will introduce some additional details about our V2X-R dataset, to help researchers using the V2X-R dataset get started quickly.



#### 7.1. Calibration of sensors

We provide calibration information for each sensor (LiDAR, 4D radar, camera) of each agent for inter-sensor fusion. In particular, the exported 4D radar point cloud has been converted to the LiDAR coordinate system of the corresponding agent in advance to facilitate fusion, so the 4D radar point cloud is referenced to the LiDAR coordinate system. If necessary, it can be converted back by the LiDAR coordinate system to the 4D radar coordinate system.

#### 7.2. Information of data

The data attributes corresponding to LiDAR, 4D radar, and camera are shown in Table 9. Both LiDAR and 4D radar sensors provide  $N \times 4$  point clouds, where  $N$  represents the number of points. It is worth noting that the 4D radar was originally exported in the CARLA simulator as an array of [azimuth, altitude, depth, velocity] in polar coordinates, which we converted to a Cartesian coordinate system. In addition, an 800x600x3 RGB image is obtained for each of the 4 cameras of each agent.

Sensor	Data Structure	File Type	Attributes
LiDAR	Point Cloud	.pcd	$N \times 4$ [ $x, y, z, intensity$ ]
4D Radar	Point Cloud	.pcd	$N \times 4$ [ $x, y, z, velocity$ ]
Camera	Image	.png	800 $\times$ 600 $\times$ 3 [ $R, G, B$ ]

Table 9. The detailed information of V2X-R data.

### 7.3. Information of data collection

Split	Seq	Name	Agent	City
Train	1	2024_06_24_19_56_04	4CAVs	Town06
	2	2024_06_24_20_24_02	2CAVs	Town06
	3	2024_06_24_21_03_22	3CAVs	Town06
	4	2024_06_24_21_23_27	2CAVs	Town06
	5	2024_06_24_21_40_16	2CAVs	Town06
	6	2024_06_24_21_46_47	1CAVs; IIInfra.	Town06
	5	2024_06_25_15_28_10	2CAVs	Town06
	8	2024_06_25_15_46_09	4CAVs	Town06
	9	2024_06_25_16_28_47	2CAVs	Town05
	10	2024_06_25_17_02_14	2CAVs	Town05
	11	2024_06_25_17_12_23	2CAVs; IIInfra.	Town05
	12	2024_06_25_18_56_34	3CAVs; IIInfra.	Town05
	13	2024_06_26_09_51_48	4CAVs	Town05
	14	2024_06_26_10_31_36	2CAVs	Town05
	15	2024_06_26_10_44_26	3CAVs	Town05
	16	2024_06_26_11_05_36	3CAVs	Town05
	17	2024_06_26_19_17_09	3CAVs; IIInfra.	Town05
	18	2024_06_26_19_38_06	2CAVs; IIInfra.	Town04
	19	2024_06_26_20_18_14	2CAVs; IIInfra.	Town05
	20	2024_06_26_21_04_51	3CAVs; IIInfra.	Town04
	21	2024_06_26_21_15_34	2CAVs; IIInfra.	Town05
	22	2024_06_26_21_22_24	2CAVs; IIInfra.	Town05
	23	2024_06_26_21_29_14	1CAVs; IIInfra.	Town04
	24	2024_06_26_21_47_03	1CAVs; IIInfra.	Town04
	25	2024_06_26_21_56_21	2CAVs; IIInfra.	Town10HD
	26	2024_06_26_22_02_55	2CAVs; IIInfra.	Town10HD
	27	2024_06_26_22_12_38	4CAVs; IIInfra.	Town10HD
	28	2024_06_26_22_18_45	3CAVs	Town10HD
	29	2024_06_26_22_30_42	2CAVs	Town07
	30	2024_06_26_22_37_45	2CAVs	Town07
	31	2024_06_27_10_09_59	3CAVs	Town07
	32	2024_06_27_11_20_21	4CAVs	Town03
	33	2024_06_27_14_22_27	3CAVs; IIInfra.	Town01
	34	2024_06_28_17_45_09	3CAVs	Town05
Validation	35	2024_06_28_18_48_16	2CAVs; IIInfra.	Town05
	36	2024_06_28_19_01_25	2CAVs; IIInfra.	Town05
	37	2024_06_28_19_20_09	2CAVs; IIInfra.	Town05
	38	2024_06_28_19_30_57	2CAVs; IIInfra.	Town10HD
	39	2024_06_28_19_45_02	5CAVs	Town02
Test	40	2024_06_27_16_27_32	2CAVs	Town06
	41	2024_06_27_17_05_43	4CAVs; IIInfra.	Town06
	42	2024_06_27_17_41_33	3CAVs	Town06
	43	2024_06_27_19_09_42	5CAVs	Town05
	44	2024_06_28_09_17_57	2CAVs	Town05
	45	2024_06_28_09_33_41	3CAVs; IIInfra.	Town05
	46	2024_06_28_09_52_03	2CAVs; IIInfra.	Town05
	47	2024_06_28_10_07_17	2CAVs; IIInfra.	Town04
	48	2024_06_28_10_22_46	2CAVs; IIInfra.	Town04
	49	2024_06_28_10_58_01	3CAVs; IIInfra.	Town10HD
	50	2024_06_28_11_17_03	3CAVs; IIInfra.	Town10HD
	51	2024_06_28_14_59_30	4CAVs	Town10HD
	52	2024_06_28_15_26_15	3CAVs	Town07
	53	2024_06_28_15_52_12	2CAVs	Town04
	54	2024_06_28_16_18_18	2CAVs	Town04
	55	2024_06_28_16_18_18	4CAVs; IIInfra.	Town03

Table 10. Information of data collection. CAVs denote Connected Automatic Vehicles and Infra. denotes Infrastructure.

Modality	Method	Epoch	Batch_size	Max_Agents	Learning_Rate	LR_Scheduler
LiDAR	V2XViT [53]	20	2	5	0.001	Multistep
	AttFuse [54]	30	4	5	0.002	Multistep
	Where2comm [12]	50	1	5	0.0002	Cosineannealwarm
	SCOPE [60]	30	2	5	0.002	Multistep
	CoBEVT [55]	30	2	5	0.001	Cosineannealwarm
	CoAlign [26]	15	2	5	0.002	Multistep
	AdaFusion [17]	30	2	5	0.0005	Multistep
	SICP [32]	20	1	5	0.001	Multistep
	MACP [27]	20	4	5	0.0002	Cosineannealwarm
	PFA-Net [50]	30	4	5	0.001	Multistep
4D Radar	RTNH [29]	15	4	5	0.001	Multistep
	V2XViT [53]	20	2	5	0.001	Multistep
	AttFuse [54]	30	4	5	0.002	Multistep
	Where2comm [12]	15	1	5	0.0002	Cosineannealwarm
	SCOPE [60]	15	2	5	0.002	Multistep
	CoBEVT [55]	30	2	5	0.001	Cosineannealwarm
	CoAlign [26]	20	2	5	0.002	Multistep
	AdaFusion [17]	15	2	5	0.0005	Multistep
	SICP [32]	20	1	5	0.001	Multistep
	InterFusion [42]	20	1	5	0.002	Multistep
LiDAR+4D Radar	L4DR [16]	30	2	5	0.002	Multistep
	V2XViT [53]	30	2	5	0.001	Multistep
	AttFuse [54]	30	2	5	0.002	Multistep
	SCOPE [60]	40	2	5	0.002	Multistep
	Where2comm [12]	30	4	5	0.0002	Cosineannealwarm
	CoBEVT [55]	40	2	5	0.001	Cosineannealwarm
	CoAlign [26]	30	2	5	0.002	Multistep
	AdaFusion [17]	40	2	5	0.0005	Multistep
	SICP [32]	20	1	5	0.001	Multistep

Table 11. Experimental parameter settings (epoch, batch\_size, max\_agent, learning\_rate, lr\_scheduler) for different modalities and methods in our benchmark section.

We summarize the critical collection details of each scene sequence by splits, as shown in Table 10, which includes agent information and scene sources for each sequence. Additional detailed acquisition information, such as the configuration of each agent’s trajectory, can be queried in the documentation of our V2X-R dataset.

## 8. Training Details of Benchmark

We also provide details about the training of all the benchmark models in the main text for researchers to refer to, as shown in Table 11. In addition, we will disclose the training profiles of all models and the pre-trained models. This can help researchers efficiently use our well-trained models on the V2X-R dataset or reproduce the same results.

## 9. Configuration of Weather Simulation

To help the reader gain a deeper understanding of the severe weather portion of the study in our V2X-R work. As shown in Table 12, we list here some important configurations for fog and snow simulations, mainly parameters used

Simulation	Parameter	Value
Fog Simulation [8]	gamma	0.000001
	alpha	0.06
	noise_variant	v2
	noise	10
	r_noise	random(1, 20)
	max_intensity	255
Snow Simulation [9]	num_intervals	64
	interval_index	random(1,64)
	snowfall_rate	0.5
	terminal_velocity	0.2
	noise_floor	0.7
	beam_divergence	0.003
	max_intensity	255

Table 12. The detailed configuration of weather simulation. The parameter names refer to the naming of the official source code and the exact meanings can be found in [8, 9].

Methods	Modality	Class	Metric	Total	Normal	Overcast	Fog	Rain	Sleet	Lightsnow	Heavysnow
AttFuse [54]	L+4DR	Sedan	$AP_{BEV}$	70.3	68.0	<b>89.4</b>	90.5	79.5	66.9	88.3	60.4
			$AP_{3D}$	69.0	66.8	79.4	88.6	70.7	59.2	<b>86.2</b>	58.6
		Bus	$AP_{BEV}$	<b>64.3</b>	<b>59.4</b>	<b>75.7</b>	-	0.4	<b>66.2</b>	80.7	70.8
			$AP_{3D}$	51.0	<b>53.3</b>	<b>75.6</b>	-	0.2	<b>65.6</b>	76.8	36.3
AttFuse w/ MDD	L+4DR	Sedan	$AP_{BEV}$	<b>76.8</b>	<b>73.8</b>	88.9	<b>90.8</b>	<b>79.7</b>	<b>68.7</b>	<b>88.4</b>	<b>61.5</b>
			$AP_{3D}$	<b>74.0</b>	<b>67.2</b>	<b>85.5</b>	<b>89.6</b>	<b>75.7</b>	<b>64.6</b>	84.5	<b>59.8</b>
		Bus	$AP_{BEV}$	64.1	55.3	72.0	-	<b>15.1</b>	62.7	<b>97.5</b>	<b>73.9</b>
			$AP_{3D}$	<b>54.6</b>	52.8	71.0	-	<b>15.0</b>	61.3	<b>85.2</b>	<b>42.6</b>

Table 13. Quantitative results of different 3D object detection methods on K-Radar dataset. We present the modality of each method (L+4DR: LiDAR-4D radar fusion) and detailed performance for each weather condition. Best in **bold**.

to adjust the level of adverse weather. Most of the other configurations implemented refer to the default configurations available on their official open-source code <sup>1</sup> <sup>2</sup>. In addition, the simulation code we implemented will be included in the publicly released code in the future.

## 10. Detailed Performance on K-Radar Dataset

### 10.1. K-Radar dataset and evaluation metrics

The K-Radar dataset [28] contains 58 sequences with 34944 frames of 64-line LiDAR, camera, and 4D radar data in various weather conditions. According to the official K-Radar split, we used 17458 frames for training and 17536 frames for testing. We adopt two evaluation metrics for 3D object detection:  $AP_{3D}$  and  $AP_{BEV}$  of the class "Sedan" and "Bus" at IoU = 0.3. We use the newest version (v2.1) of the label.

### 10.2. Performance on various weather.

To further demonstrate the performance improvement of our MDD module in various real-world adverse weather conditions. We provide more detailed results on the K-Radar real adverse weather dataset rather than just the average of adverse weather. As shown in Table 13, with the addition of our MDD module, AttFuse first of all got a big boost in Total basically (except for Bus's  $AP_{BEV}$ ). Under the Sedan class, there are significant improvements in every weather except Overcast which is similar, especially in 6.1  $AP_{3D}$ @Overcast and 5.4  $AP_{3D}$ @Sleet performance improvements. In addition, the results of the Bus class are well worth exploring. We find significant decreases in Normal, Overcast, and Sleet, but very significant increases in Rain, Lightsnow, and Heavysnow. We assert this is due to the nature of the larger 3D bounding boxes of the Bus class, which is particularly sensitive to the denoising module, causing a drop in some weather and a significant rise in others. Overall, however, the Total performance on the Bus class remains suggestive. These detailed analyses fur-

Component	Parameter	Value
Denoiser (U-net)	input_channel	128
	mid_channel	128
	timestep_channel	64
	output_channel	64
	number_layers	2
	number_resblock	2
Diffusion Process	timesteps	3
	betas	[0.005,0.0275,0.05]

Table 14. The implementation details of our MDD module.

ther validate the effectiveness of our MDD module under real-world conditions.

## 11. Implementation of MDD

Here, we will provide a concrete implementation of the MDD module. It comprises a denoiser network with a U-net [35] structure and a diffusion process. Some important parameter settings are shown in Table 14.

## 12. Visualization of V2X-R Dataset

Finally, in order to visually intuitively verify the realism of the simulated LiDAR-4D radar data on our V2X-R dataset and the advantages of the cooperative LiDAR-4D radar point cloud. We have visualized and compared the simulated LiDAR-4D radar point cloud on our V2X-R dataset with the real LiDAR-4D radar point cloud on the VoD dataset [30]. As shown in Fig. 6, it can be found that our simulated LiDAR-4D radar point cloud has a certain degree of realism. This proves the value of conducting 4D radar-related research on our V2X-R dataset. Meanwhile, by comparing the real single-agent 4D radar with the multi-agent 4D radar, it can be found that the multi-agent collaborative 4D radar has a significantly higher resolution. As we introduced in the Introduction section of the main text, the multi-agent cooperative 4D radar has a certain independent perception ability.

<sup>1</sup>Fog Simulation Code

<sup>2</sup>Snow Simulation Code

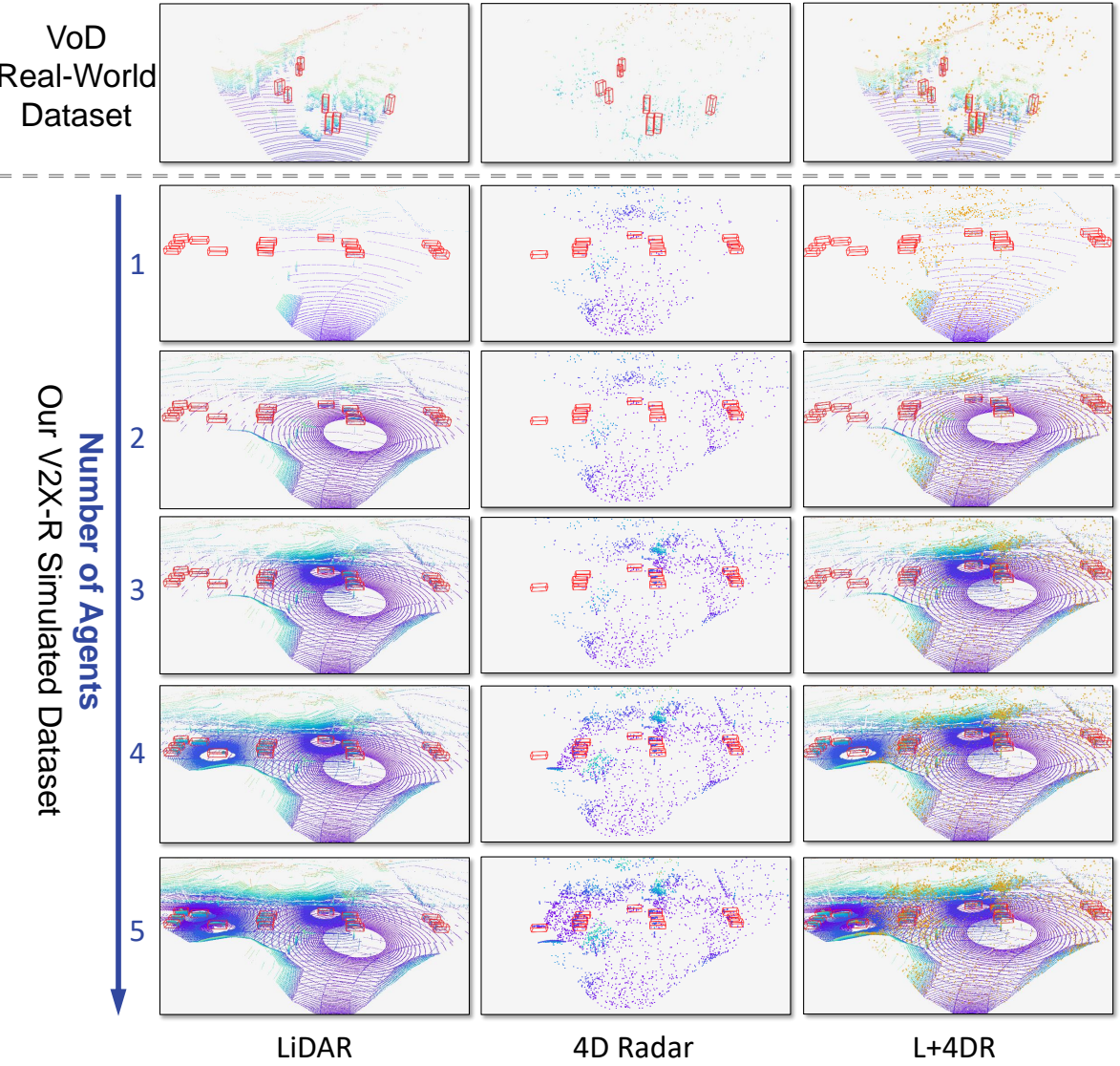


Figure 6. Visualization of our V2X-R dataset and VoD [30] real-world dataset. The L+4DR in the last column indicates that the LiDAR point cloud is visualized together with the 4D radar point cloud, where to distinguish between them, we use colored dots (slightly smaller) for the LiDAR point cloud and orange dots (slightly larger) for the 4D radar point cloud. Color point clouds are assigned by z-axis values.

## References

- [1] Jujeong Chae, Hyeonseong Kim, and Kuk-Jin Yoon. Towards robust 3d object detection with lidar and 4d radar fusion in various weather conditions. In *CVPR*, pages 15162–15172, 2024. [1](#), [2](#), [5](#)
- [2] Qi Chen, Sihai Tang, Qing Yang, and Song Fu. Cooperative perception for connected autonomous vehicles based on 3d point clouds. *Cornell University - arXiv, Cornell University - arXiv*, 2019. [3](#)
- [3] Jiajun Deng, Shaoshuai Shi, Peiwei Li, Wengang Zhou, Yanyong Zhang, and Houqiang Li. Voxel R-CNN: Towards High Performance Voxel-based 3D Object Detection. *AAAI*, 35, 2021. [2](#)
- [4] Jinhao Deng, Wei Ye, Hai Wu, Xun Huang, Qiming Xia, Xin Li, Jin Fang, Wei Li, Chenglu Wen, and Cheng Wang. Cmd: A cross mechanism domain adaptation dataset for 3d object detection. In *European Conference on Computer Vision*, pages 219–236. Springer, 2025. [1](#)
- [5] Yinpeng Dong, Caixin Kang, Jinlai Zhang, Zijian Zhu, Yikai Wang, Xiao Yang, Hang Su, Xingxing Wei, and Jun Zhu. Benchmarking robustness of 3d object detection to common corruptions. In *Proceedings of the IEEE/CVF Conference on Computer Vision and Pattern Recognition*, pages 1022–1032, 2023. [3](#)
- [6] Alexey Dosovitskiy, German Ros, Felipe Codevilla, Anto-

nio Lopez, and Vladlen Koltun. Carla: An open urban driving simulator. In *Conference on robot learning*, pages 1–16. PMLR, 2017. 3

[7] Ahmed Ghita, Bjørk Antoniussen, Walter Zimmer, Ross Greer, Christian Creß, Andreas Møgelmose, Mohan M Trivedi, and Alois C Knoll. Activeanno3d—an active learning framework for multi-modal 3d object detection. *arXiv preprint arXiv:2402.03235*, 2024. 2

[8] Martin Hahner, Christos Sakaridis, Dengxin Dai, and Luc Van Gool. Fog Simulation on Real LiDAR Point Clouds for 3D Object Detection in Adverse Weather. In *ICCV*, 2021. 1, 2, 3, 10

[9] Martin Hahner, Christos Sakaridis, Mario Bijelic, Felix Heide, Fisher Yu, Dengxin Dai, and Luc Van Gool. LiDAR Snowfall Simulation for Robust 3D Object Detection. In *CVPR*, 2022. 1, 3, 10

[10] Z Han, J Wang, Z Xu, S Yang, L He, S Xu, and J Wang. 4d millimeter-wave radar in autonomous driving: A survey. *arxiv* 2023. *arXiv preprint arXiv:2306.04242*, 2023. 1

[11] Jonathan Ho, Ajay Jain, and Pieter Abbeel. Denoising diffusion probabilistic models. *Advances in neural information processing systems*, 33:6840–6851, 2020. 5

[12] Yue Hu, Shaoheng Fang, Zixing Lei, Yiqi Zhong, and Siheng Chen. Where2comm: Communication-efficient collaborative perception via spatial confidence maps. *Advances in neural information processing systems*, 35:4874–4886, 2022. 1, 3, 5, 6, 7, 10

[13] Yue Hu, Juntong Peng, Sifei Liu, Junhao Ge, Si Liu, and Siheng Chen. Communication-efficient collaborative perception via information filling with codebook. In *CVPR*, pages 15481–15490, 2024. 1, 3

[14] Kuan-Chih Huang, Weijie Lyu, Ming-Hsuan Yang, and Yi-Hsuan Tsai. Ptt: Point-trajectory transformer for efficient temporal 3d object detection. In *CVPR*, pages 14938–14947, 2024. 1

[15] Xun Huang, Hai Wu, Xin Li, Xiaoliang Fan, Chenglu Wen, and Cheng Wang. Sunshine to rainstorm: Cross-weather knowledge distillation for robust 3d object detection. In *AAAI*, pages 2409–2416, 2024. 1, 2

[16] Xun Huang, Ziyu Xu, Hai Wu, Jinlong Wang, Qiming Xia, Yan Xia, Jonathan Li, Kyle Gao, Chenglu Wen, and Cheng Wang. L4dr: Lidar-4dradar fusion for weather-robust 3d object detection. *arXiv preprint arXiv:2408.03677*, 2024. 1, 2, 5, 6, 7, 10

[17] Haowen Lai, Peng Yin, and Sebastian Scherer. Adafusion: Visual-lidar fusion with adaptive weights for place recognition. *IEEE Robotics and Automation Letters*, 7(4):12038–12045, 2022. 6, 7, 10

[18] Alex H. Lang, Sourabh Vora, Holger Caesar, Lubing Zhou, Jiong Yang, and Oscar Beijbom. Pointpillars: Fast encoders for object detection from point clouds. In *2019 IEEE/CVF Conference on Computer Vision and Pattern Recognition*, pages 12689–12697, 2019. 2

[19] Yiming Li, Dekun Ma, Ziyuan An, Zixun Wang, Yiqi Zhong, Siheng Chen, and Chen Feng. V2x-sim: Multi-agent collaborative perception dataset and benchmark for autonomous driving. *IEEE Robotics and Automation Letters*, 7(4):10914–10921, 2022. 3

[20] Yingwei Li, Adams Wei Yu, Tianjian Meng, Ben Caine, Ji-quan Ngiam, Daiyi Peng, Junyang Shen, Yifeng Lu, Denny Zhou, Quoc V. Le, Alan Yuille, and Mingxing Tan. Deep-fusion: Lidar-camera deep fusion for multi-modal 3d object detection. In *CVPR*, pages 17182–17191, 2022. 2

[21] Yu-Jhe Li, Jinhyung Park, Matthew O’Toole, and Kris Kitani. Modality-agnostic learning for radar-lidar fusion in vehicle detection. In *CVPR*, pages 918–927, 2022. 2

[22] Yu-Jhe Li, Matthew O’Toole, and Kris Kitani. St-mvdnet++: Improve vehicle detection with lidar-radar geometrical augmentation via self-training. In *ICASSP 2023-2023 IEEE International Conference on Acoustics, Speech and Signal Processing (ICASSP)*, pages 1–5. IEEE, 2023. 2

[23] Jia Lin, Huilin Yin, Jun Yan, Wancheng Ge, Hao Zhang, and Gerhard Rigoll. Improved 3D Object Detector Under Snowfall Weather Condition Based on LiDAR Point Cloud. *IEEE Sensors Journal*, 22, 2022. 2

[24] Zhijian Liu, Haotian Tang, Alexander Amini, Xinyu Yang, Huizi Mao, Daniela L. Rus, and Song Han. Bevfusion: Multi-task multi-sensor fusion with unified bird’s-eye view representation. In *2023 IEEE International Conference on Robotics and Automation (ICRA)*, pages 2774–2781, 2023. 1, 2

[25] Pablo Alvarez Lopez, Michael Behrisch, Laura Bieker-Walz, Jakob Erdmann, Yun-Pang Flötteröd, Robert Hilbrich, Leonhard Lücken, Johannes Rummel, Peter Wagner, and Eva-marie Wiessner. Microscopic traffic simulation using sumo. In *2018 21st International Conference on Intelligent Transportation Systems (ITSC)*, pages 2575–2582, 2018. 3

[26] Yifan Lu, Quanhao Li, Baoan Liu, Mehrdad Dianati, Chen Feng, Siheng Chen, and Yanfeng Wang. Robust collaborative 3d object detection in presence of pose errors. In *2023 IEEE International Conference on Robotics and Automation (ICRA)*, pages 4812–4818, 2023. 6, 7, 10

[27] Yunsheng Ma, Juanwu Lu, Can Cui, Sicheng Zhao, Xu Cao, Wenqian Ye, and Ziran Wang. Macp: Efficient model adaptation for cooperative perception. In *2024 IEEE/CVF Winter Conference on Applications of Computer Vision (WACV)*, pages 3361–3370, 2024. 6, 10

[28] Dong-Hee Paek, Seung-Hyun Kong, and Kevin Tirta Wijaya. K-radar: 4d radar object detection for autonomous driving in various weather conditions. *Advances in Neural Information Processing Systems*, 35:3819–3829, 2022. 6, 8, 11

[29] Dong-Hee Paek, SEUNG-HYUN KONG, and Kevin Tirta Wijaya. K-radar: 4d radar object detection for autonomous driving in various weather conditions. In *Advances in Neural Information Processing Systems*, pages 3819–3829. Curran Associates, Inc., 2022. 6, 10

[30] Andras Palfy, Ewoud Pool, Srimannarayana Baratam, Julian FP Kooij, and Dariu M Gavrila. Multi-class road user detection with 3+ 1d radar in the view-of-delft dataset. *IEEE Robotics and Automation Letters*, 7(2):4961–4968, 2022. 11, 12

[31] Kun Qian, Shilin Zhu, Xinyu Zhang, and Li Erran Li. Robust multimodal vehicle detection in foggy weather using complementary lidar and radar signals. In *CVPR*, pages 444–453, 2021. 2, 3

[32] Deyuan Qu, Qi Chen, Tianyu Bai, Hongsheng Lu, Heng Fan, Hao Zhang, Song Fu, and Qing Yang. Sicip: Simultaneous individual and cooperative perception for 3d object detection in connected and automated vehicles, 2024. 1, 5, 6, 7, 10

[33] Andreas Rauch, Felix Klanner, Ralph Rasshofer, and Klaus Dietmayer. Car2x-based perception in a high-level fusion architecture for cooperative perception systems. In *2012 IEEE Intelligent Vehicles Symposium*, 2012. 3

[34] Zaydoun Yahya Rawashdeh and Zheng Wang. Collaborative automated driving: A machine learning-based method to enhance the accuracy of shared information. In *2018 21st International Conference on Intelligent Transportation Systems (ITSC)*, 2018. 3

[35] Olaf Ronneberger, Philipp Fischer, and Thomas Brox. U-net: Convolutional networks for biomedical image segmentation. In *Medical image computing and computer-assisted intervention–MICCAI 2015: 18th international conference, Munich, Germany, October 5–9, 2015, proceedings, part III* 18, pages 234–241. Springer, 2015. 5, 11

[36] Shaoshuai Shi, Chaoxu Guo, Li Jiang, Zhe Wang, Jianping Shi, Xiaogang Wang, and Hongsheng Li. PV-RCNN: Point-Voxel Feature Set Abstraction for 3D Object Detection. In *CVPR*, 2020. 2

[37] Shaoshuai Shi, Li Jiang, Jiajun Deng, Zhe Wang, Chaoxu Guo, Jianping Shi, Xiaogang Wang, and Hongsheng Li. PV-RCNN++: Point-Voxel Feature Set Abstraction With Local Vector Representation for 3D Object Detection. *Int. J. Comput. Vision*, 131, 2022. 2

[38] Jingyu Song, Lingjun Zhao, and Katherine A Skinner. Lira-fusion: Deep adaptive lidar-radar fusion for 3d object detection. *arXiv preprint arXiv:2402.11735*, 2024. 2

[39] Shunqiao Sun and Yimin D Zhang. 4d automotive radar sensing for autonomous vehicles: A sparsity-oriented approach. *IEEE Journal of Selected Topics in Signal Processing*, 15(4): 879–891, 2021. 1

[40] Haiyang Wang, Chen Shi, Shaoshuai Shi, Meng Lei, Sen Wang, Di He, Bernt Schiele, and Liwei Wang. DSVT: Dynamic Sparse Voxel Transformer With Rotated Sets. In *CVPR*, 2023. 2

[41] Li Wang, Xinyu Zhang, Jun Li, Baowei Xv, Rong Fu, Haifeng Chen, Lei Yang, Dafeng Jin, and Lijun Zhao. Multi-modal and multi-scale fusion 3d object detection of 4d radar and lidar for autonomous driving. *IEEE Transactions on Vehicular Technology*, 2022. 1, 2, 5

[42] Li Wang, Xinyu Zhang, Baowei Xv, Jinzhao Zhang, Rong Fu, Xiaoyu Wang, Lei Zhu, Haibing Ren, Pingping Lu, Jun Li, and Huaping Liu. Interfusion: Interaction-based 4d radar and lidar fusion for 3d object detection. In *2022 IEEE/RSJ International Conference on Intelligent Robots and Systems (IROS)*, pages 12247–12253, 2022. 1, 2, 5, 6, 7, 10

[43] Hai Wu, Chenglu Wen, Wei Li, Xin Li, Ruigang Yang, and Cheng Wang. Transformation-equivariant 3d object detection for autonomous driving. In *AAAI*, pages 2795–2802, 2023. 2

[44] Hai Wu, Chenglu Wen, Shaoshuai Shi, Xin Li, and Cheng Wang. Virtual Sparse Convolution for Multimodal 3D Object Detection. In *CVPR*, 2023. 2

[45] Hai Wu, Shijia Zhao, Xun Huang, Chenglu Wen, Xin Li, and Cheng Wang. Commonsense prototype for outdoor unsupervised 3d object detection. *arXiv preprint arXiv:2404.16493*, 2024. 1

[46] Qiming Xia, Jinhao Deng, Chenglu Wen, Hai Wu, Shaoshuai Shi, Xin Li, and Cheng Wang. Coin: Contrastive instance feature mining for outdoor 3d object detection with very limited annotations. In *Proceedings of the IEEE/CVF International Conference on Computer Vision (ICCV)*, pages 6254–6263, 2023. 2

[47] Qiming Xia, Wei Ye, Hai Wu, Shijia Zhao, Leyuan Xing, Xun Huang, Jinhao Deng, Xin Li, Chenglu Wen, and Cheng Wang. Hinted: Hard instance enhanced detector with mixed-density feature fusion for sparsely-supervised 3d object detection. In *CVPR*, pages 15321–15330, 2024. 2

[48] Hao Xiang, Runsheng Xu, and Jiaqi Ma. Hm-vit: Heteromodal vehicle-to-vehicle cooperative perception with vision transformer. In *Proceedings of the IEEE/CVF International Conference on Computer Vision*, pages 284–295, 2023. 1

[49] Baowei Xu, Xinyu Zhang, Li Wang, Xiaomei Hu, Zhiwei Li, Shuyue Pan, Jun Li, and Yongqiang Deng. Rpfa-net: a 4d radar pillar feature attention network for 3d object detection. In *2021 IEEE International Intelligent Transportation Systems Conference (ITSC)*, pages 3061–3066, 2021. 6

[50] Baowei Xu, Xinyu Zhang, Li Wang, Xiaomei Hu, Zhiwei Li, Shuyue Pan, Jun Li, and Yongqiang Deng. Rpfa-net: a 4d radar pillar feature attention network for 3d object detection. In *2021 IEEE International Intelligent Transportation Systems Conference (ITSC)*, pages 3061–3066, 2021. 6, 10

[51] Ge Xu, Amir Khan, Ata Jahangir Moshayedi, Xiaohong Zhang, and Yang Shuxin. The object detection, perspective and obstacles in robotic: A review. *EAI Endorsed Transactions on AI and Robotics*, 1:7–15, 2022. 2

[52] Runsheng Xu, Yi Guo, Xu Han, Xin Xia, Hao Xiang, and Jiaqi Ma. Opencka: an open cooperative driving automation framework integrated with co-simulation. In *2021 IEEE International Intelligent Transportation Systems Conference (ITSC)*, pages 1155–1162. IEEE, 2021. 3

[53] Runsheng Xu, Hao Xiang, Zhengzhong Tu, Xin Xia, Ming-Hsuan Yang, and Jiaqi Ma. V2x-vit: Vehicle-to-everything cooperative perception with vision transformer. In *European conference on computer vision*, pages 107–124. Springer, 2022. 1, 3, 5, 6, 7, 10

[54] Runsheng Xu, Hao Xiang, Xin Xia, Xu Han, Jinlong Li, and Jiaqi Ma. Opv2v: An open benchmark dataset and fusion pipeline for perception with vehicle-to-vehicle communication. In *2022 International Conference on Robotics and Automation (ICRA)*, pages 2583–2589. IEEE, 2022. 1, 2, 3, 6, 7, 8, 10, 11

[55] Runsheng Xu, Zhengzhong Tu, Hao Xiang, Wei Shao, Bolei Zhou, and Jiaqi Ma. Cobevt: Cooperative bird’s eye view semantic segmentation with sparse transformers. In *Conference on Robot Learning*, pages 989–1000. PMLR, 2023. 1, 3, 5, 6, 7, 10

[56] Runsheng Xu, Xin Xia, Jinlong Li, Hanzhao Li, Shuo Zhang, Zhengzhong Tu, Zonglin Meng, Hao Xiang, Xiaoyu Dong, Rui Song, Hongkai Yu, Bolei Zhou, and Jiaqi Ma. V2v4real:

A real-world large-scale dataset for vehicle-to-vehicle cooperative perception. In *CVPR*, pages 13712–13722, 2023. 3

[57] Runsheng Xu, Xin Xia, Jinlong Li, Hanzhao Li, Shuo Zhang, Zhengzhong Tu, Zonglin Meng, Hao Xiang, Xiaoyu Dong, Rui Song, et al. V2v4real: A real-world large-scale dataset for vehicle-to-vehicle cooperative perception. In *CVPR*, pages 13712–13722, 2023. 1

[58] Junjie Yan, Yingfei Liu, Jianjian Sun, Fan Jia, Shuailin Li, Tiancai Wang, and Xiangyu Zhang. Cross modal transformer: Towards fast and robust 3d object detection. In *Proceedings of the IEEE/CVF International Conference on Computer Vision*, pages 18268–18278, 2023. 2

[59] Yan Yan, Yuxing Mao, and Bo Li. SECOND: Sparsely Embedded Convolutional Detection. *Sensors*, 18, 2018. 2

[60] Kun Yang, Dingkang Yang, Jingyu Zhang, Mingcheng Li, Yang Liu, Jing Liu, Hanqi Wang, Peng Sun, and Liang Song. Spatio-temporal domain awareness for multi-agent collaborative perception. In *Proceedings of the IEEE/CVF International Conference on Computer Vision*, pages 23383–23392, 2023. 1, 3, 6, 7, 10

[61] Zetong Yang, Yanan Sun, Shu Liu, and Jiaya Jia. 3DSSD: Point-Based 3D Single Stage Object Detector. In *CVPR*, 2020. 2

[62] Hanrong Ye and Dan Xu. Diffusionmtl: Learning multi-task denoising diffusion model from partially annotated data. In *Proceedings of the IEEE/CVF Conference on Computer Vision and Pattern Recognition*, pages 27960–27969, 2024. 5

[63] Haibao Yu, Yizhen Luo, Mao Shu, Yiyi Huo, Zebang Yang, Yifeng Shi, Zhenglong Guo, Hanyu Li, Xing Hu, Jirui Yuan, and Zaiqing Nie. Dair-v2x: A large-scale dataset for vehicle-infrastructure cooperative 3d object detection. 2022. 3

[64] Haibao Yu, Yizhen Luo, Mao Shu, Yiyi Huo, Zebang Yang, Yifeng Shi, Zhenglong Guo, Hanyu Li, Xing Hu, Jirui Yuan, et al. Dair-v2x: A large-scale dataset for vehicle-infrastructure cooperative 3d object detection. In *CVPR*, pages 21361–21370, 2022. 1

[65] Gang Zhang, Junnan Chen, Guohuan Gao, Jianmin Li, Si Liu, and Xiaolin Hu. Safdnet: A simple and effective network for fully sparse 3d object detection. In *CVPR*, pages 14477–14486, 2024. 1, 2

[66] Binyu Zhao, Wei ZHANG, and Zhaonian Zou. Bm2cp: Efficient collaborative perception with lidar-camera modalities. In *Conference on Robot Learning*, pages 1022–1035. PMLR, 2023. 1, 3

[67] Lianqing Zheng, Sen Li, Bin Tan, Long Yang, Sihan Chen, Libo Huang, Jie Bai, Xichan Zhu, and Zhixiong Ma. Rcfusion: Fusing 4-d radar and camera with bird's-eye view features for 3-d object detection. *IEEE Transactions on Instrumentation and Measurement*, 72:1–14, 2023. 1

[68] Walter Zimmer, Gerhard Arya Wardana, Suren Sritharan, Xingcheng Zhou, Rui Song, and Alois C Knoll. Tumtraf v2x cooperative perception dataset. In *CVPR*, pages 22668–22677, 2024. 1